mater.scichina.com link.springer.com
Published online 25 November 2022 | https://doi.org/10.1007/s40843-022-2244-y
Sci China Mater 2023, 66(3): 1157–1164

Trap-mediated bipolar charge transport in NiO/Ga_2O_3 p^+-n heterojunction power diodes

Zhengpeng Wang[1], He-He Gong[1], Xin-Xin Yu[1], Xiaoli Ji[1], Fang-Fang Ren[1], Yi Yang[1], Shulin Gu[1], Youdou Zheng[1], Rong Zhang[1] and Jiandong Ye[1,2*]

ABSTRACT **The construction of p-NiO/n-Ga_2O_3 heterojunction becomes a popular alternative to overcome the technological bottleneck of p-type Ga_2O_3 for developing bipolar power devices for practical applications, whereas the identification of performance-limiting traps and the bipolar transport dynamics are still not exploited yet. To this end, the fundamental correlation of carrier transport, trapping and recombination kinetics in NiO/β-Ga_2O_3 p^+-n heterojunction power diodes has been investigated. The quantitative modeling of the temperature-dependent current-voltage characteristics indicates that the modified Shockley-Read-Hall recombination mediated by majority carrier trap states with an activation energy of 0.64 eV dominates the trap-assisted tunneling process in the forward subthreshold conduction regime, while the minority carrier diffusion with near-unity ideality factors is overwhelming at the bias over the turn-on voltage. The leakage mechanism at high reverse biases is governed by the Poole-Frenkel emissions through the β-Ga_2O_3 bulk traps with a barrier height of 0.75 eV, which is supported by the identification of majority bulk traps with the energy level of E_C − 0.75 eV through the isothermal capacitance transient spectroscopic analysis. These findings bridge the knowledge gap between bipolar charge transport and deep-level trap behaviors in Ga_2O_3, which is crucial to understand the reliability of Ga_2O_3 bipolar power rectifiers.**

Keywords: ultra-wide bandgap semiconductors, bipolar charge transport, capacitance transient spectroscopy

INTRODUCTION

Beta-phase gallium oxide (β-Ga_2O_3) has invoked great interest for power device applications beyond existing technologies [1,2]. With superior properties, bipolar power devices based on β-Ga_2O_3 are highly desirable for high-power electronic applications [3–5]. To date, the technical progress of Ga_2O_3 power diodes is now stuck at a critical point where a lack of p-type Ga_2O_3 seriously limits their further development and even future commercialization. To overcome the technological bottleneck, an alternative strategy to realize bipolar devices is the construction of p-n heterojunction with foreign p-type materials [6–9]. Recently, we have demonstrated NiO/β-Ga_2O_3 p-n heterojunction power diodes (HJD) with superior performances that outperform the unipolar counterpart, Schottky barrier diode (SBD) [7,10,11]. Despite these promises, no matter what terminal structure is employed, the theoretical power figure-of-merits (FOM) of β-Ga_2O_3 is still far from being reached due to the existence of deep-level traps distributed at interfaces or within the bulk drift layer. Deep-level traps in β-Ga_2O_3 have been reported as the origin of the reverse leakage pathway of premature breakdown and the dominant source of threshold voltage instability of metal-semiconductor field effect transistors (MESFETs) [10,12–15], which leads to the undesirable device performances. In particular, the reported all-oxide heterojunctions with type-II band alignments usually exhibit non-unity ideality factors and the abnormal subthreshold "turn-on" characteristics [6,9,16–18]. Therefore, trap-mediated transport dynamics in the p-n heterojunction are crucial for the comprehensive evaluation of β-Ga_2O_3 bipolar power devices, which is not fully explored yet. With this motivation, the dominant majority and minority carrier traps in unintentionally doped (UID) β-Ga_2O_3 have been identified by means of deep-level transient spectroscopy (DLTS) and isothermal capacitance transient spectroscopy (ICTS). The correlated trap-limited transport mechanisms in the subthreshold conduction regime of the NiO/β-Ga_2O_3 p-n heterojunction have been quantitatively investigated, which is crucial to understand the reliability degradation of Ga_2O_3 power rectifiers, and is also important guidance for the material quality optimization and device performance improvement.

EXPERIMENTAL SECTION

The NiO/β-Ga_2O_3 p-n HJDs were fabricated on a 650-μm-thick UID β-Ga_2O_3 (−201) bulk crystal and the referenced Ni/β-Ga_2O_3 SBDs were also produced on the identical β-Ga_2O_3 wafer. The 5 mm × 5 mm UID β-Ga_2O_3 (−201) substrate used in this work was diced from a commercial 2-inch wafer, which is a commercial substrate purchased from Tamura Corporation, Japan. It was grown by an edge-defined film-fed growth (EFG) method and chemically mechanically polished (CMP) on the front side. Fig. 1a shows the cross-sectional schematics of Ni/β-Ga_2O_3 SBD and NiO/β-Ga_2O_3 HJD. Prior to the Ohmic contact deposition, the photoresist has been used to cover the wafer-front side to prevent any unintentional contamination. Subsequently, the fabrication of both diodes commenced with the full-area back Ohmic contact of Ti/Au (200/100 nm), which was deposited by electron beam evaporation (EBE). The cleaning processes with acetone, ethanol, and deionized water in sequence were then

[1] School of Electronic Science and Engineering, Nanjing University, Nanjing 210023, China
[2] Shenzhen Research Institute of Shandong University, Shenzhen 518000, China
[*] Corresponding author (email: yejd@nju.edu.cn)

© Science China Press and Springer-Verlag GmbH Germany, part of Springer Nature 2022

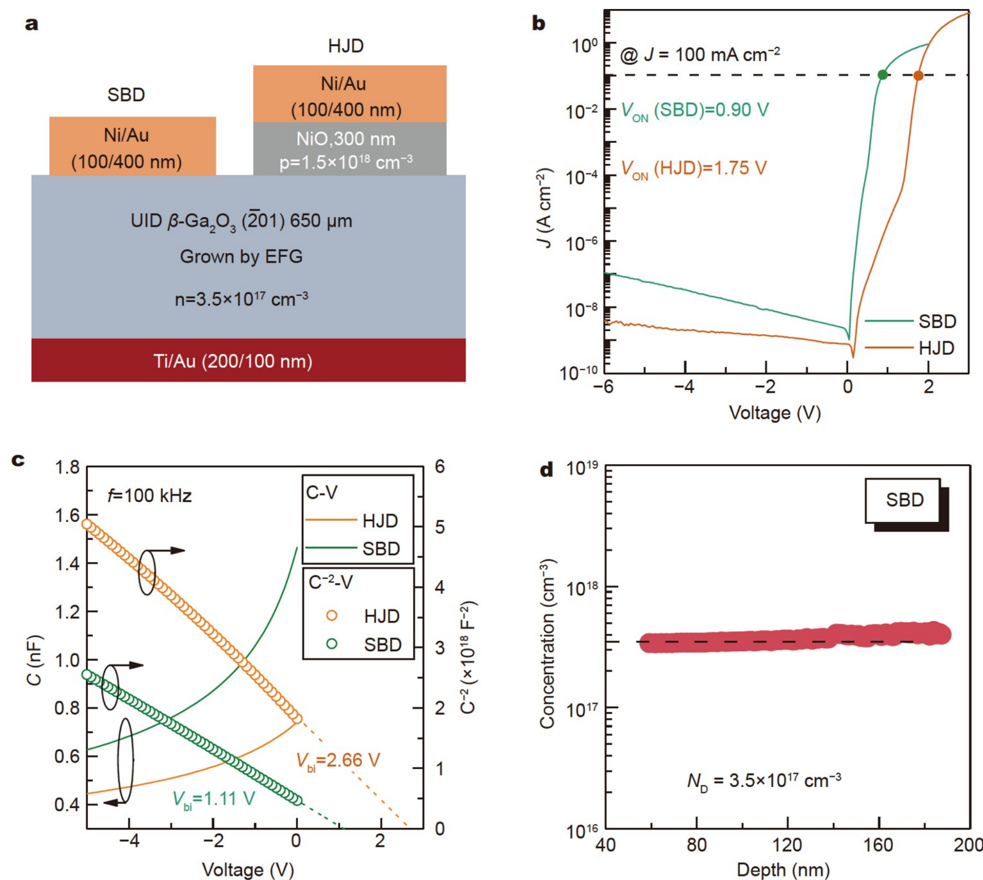

Figure 1 (a) Cross-sectional schematics, (b) semi-logarithmic *J-V*, (c) *C-V* and $1/C^{-2}$-*V* characteristics of Ni/β-Ga_2O_3 SBD and NiO/β-Ga_2O_3 HJD. (d) The depth-profile of carrier concentration in the β-Ga_2O_3 bulk.

performed to remove the covered photoresist on the front side. Then, a rapid thermal annealing (RTA) process was then performed at 470°C in N_2 ambient for 1 min to reduce the Ohmic contact resistance. Subsequently, the 1 mm ×1 mm squared NiO layer with a thickness of 300 nm was selectively grown by radio frequency (RF) magnetron sputtering technique at room temperature (RT) on the patterned β-Ga_2O_3 utilizing a shadow mask. The RF power was 50 W and the used target was high-purity (99.99%) NiO ceramic. The growth pressure was 0.6 Pa with an Ar/O_2 flux ratio of 3:1. Finally, Ni/Au (100/400 nm) metal stack was deposited upon p-NiO by EBE with good Ohmic features, which also served as the Schottky contact for the SBD counterpart. Current-voltage (*I-V*) and capacitance-voltage (*C-V*) characteristics were measured using a Keithley 2634B current source meter and a Keysight E4980A LCR meter, respectively. DLTS and ICTS measurements were carried out using a lock-in amplifier Deep Level Spectrometer (Semilab, DLS83D).

RESULTS

Fig. 1b shows the semi-logarithmic current *J-V* characteristics of both diodes measured at RT. The reverse current density is reduced remarkably from 1.11×10^{-7} A cm^{-2} for the SBD down to 3.94×10^{-9} A cm^{-2} for the HJD device at −6 V. The turn-on voltage (V_{ON}) is defined as the applied bias at the forward current density level of J = 100 mA cm^{-2}, which is 0.90 and 1.75 V, respectively, for the SBD and HJD devices. Note that, the forward S-shaped *J-V* kink characteristic is distinct for the HJD with the current kink-point corresponding to the V_{ON}, which has been widely reported in heterojunction solar cells and field effect transistors [19,20]. It suggests that carrier capture and emission processes *via* deep-level traps are driven by various external stresses, such as electric bias and/or temperature, which govern the carrier transport kinetics and the stability of device performance.

Fig. 1c shows *C-V* and C^{-2}-*V* characteristics of both diodes measured at 100 kHz. The built-in potentials (V_{bi}) of SBD and HJD are determined to be 1.11 and 2.66 V, respectively, which are slightly larger than their V_{ON}. This may be associated with the inhomogeneity of the potential barrier within the large electrode region (1 mm × 1 mm) [7] and the trap-mediated electron transport processes [21]. Determined from the differential slope of $1/C^2$-*V* plot of the SBD, the depth-profile of net donor concentration (N_D) in bulk β-Ga_2O_3 is uniform with an average value of 3.5×10^{17} cm^{-3}, as shown in Fig. 1d. Consequently, the average acceptor concentration (N_A) in the NiO side is obtained to be 1.5×10^{18} cm^{-3} in terms of $C = [q\varepsilon_0\varepsilon_n\varepsilon_p N_D N_A/2(\varepsilon_n N_D + \varepsilon_p N_A)]^{1/2}(V_{bi} - V_A)^{-1/2}$ [22], where q is the electron charge, $\varepsilon_n = 10$ and $\varepsilon_p = 9.1$ are the static dielectric permittivity of β-Ga_2O_3 [23] and NiO [24], respectively, ε_0 is the vacuum permittivity, V_{bi} = 2.66 V for HJD, and V_A is the applied voltage. Considering the magnitude difference between N_D and N_A, the NiO/β-Ga_2O_3 HJD can be regarded as a p^+-n heterojunction, and the space charge region (SCR) is mainly extended into the

 © Science China Press and Springer-Verlag GmbH Germany, part of Springer Nature 2022

β-Ga_2O_3 side.

Fig. 2a shows the temperature-dependent forward current-voltage (J-V-T) characteristics of HJD ranging from 300 to 548 K plotted in a semi-logarithmic scale. Overall, all the curves exhibit distinct S-shaped current kink features, and two successive segments with different subthreshold slopes (SS) are observed, which are denoted as regions I and II. With elevated temperatures, a rigid leftward-shift of the J-V characteristic is observed in the forward subthreshold region. It has originated from the reduced built-in potential owing to the shrinkage of material bandgaps, which is also consistent with the decreased V_{ON} from 1.75 V at 300 K to 1.26 V at 548 K, as shown in Fig. S1. The forward current density in region-II tends to saturate as T > 498 K, while its subthreshold slopes are almost insensitive to temperature, which is one of the typical signs of trap-assisted tunneling (TAT) at the subthreshold conduction regime [25]. Fig. 2c shows the bias-dependent ideality factors (η) that are extracted from the differential Shockley equation of

$$\partial V/\partial \ln(J) = \eta kT/q + JR_S, \quad (1)$$

where R_S is the series resistance [26]. Each individual S-shaped η-V curve shows an obvious peak (η > 2) at region-II and a minimal value as the bias approaches the kink voltage, while a large η value at a high forward bias is induced by the series resistance effect [27]. The non-unity of η in the subthreshold region indicates that other competitive conduction mechanisms (η > 1) related to traps/defects are overwhelming the minority carrier diffusion (η = 1) [28,29].

By assuming the characteristic energy $E_0 = \eta kT$ [25,30], the dominant transport mechanism can be judged based on the η variation, as summarized in Fig. 2b. With temperature increasing from 300 to 498 K, the peak value of η (η_{max}) decreases from 7.5 to 4.5, and E_0 exhibits small thermal variation with an average value of 182 meV, both of which are strong indicators of the TAT process that governs the subthreshold conduction [25,30]. In general, the characteristic energy E_0 is related to the transparency of the barrier encountered by the tunneling particles during the TAT process [25,30],

$$E_0 = \frac{4qh}{\pi}\sqrt{\frac{N_{SC}}{m_e^* \varepsilon_n \varepsilon_0}}, \quad (2)$$

where h is the Planck constant, $N_{SC} \approx N_D$ is the reduced doping concentration at the SCR edges [30], and $m_e^* = 0.23m_0$ is the electron effective mass of β-Ga_2O_3 [31]. Considering the facts that the background electron concentration in the UID β-Ga_2O_3 bulk is somewhat inhomogeneous and the electron effective mass is dependent on the electron concentration, the calculated E_0 (116 meV) is roughly consistent with the experimental value. In the widely accepted Hurkx's model, the TAT process can be described by the modified Shockley-Read-Hall (SRH) recombination model with an electric field-dependent reduction of carrier lifetimes [32]. Furthermore, the minimal η (η_{min}) value decreases from 1.40 at 300 K to 1.15 at 548 K and the entire η-V curves exhibit the similar leftward-shift with elevated temperatures. It suggests that the minority carrier diffusion is more competitive with elevated temperatures and governs the carrier transport at high forward biases in region I.

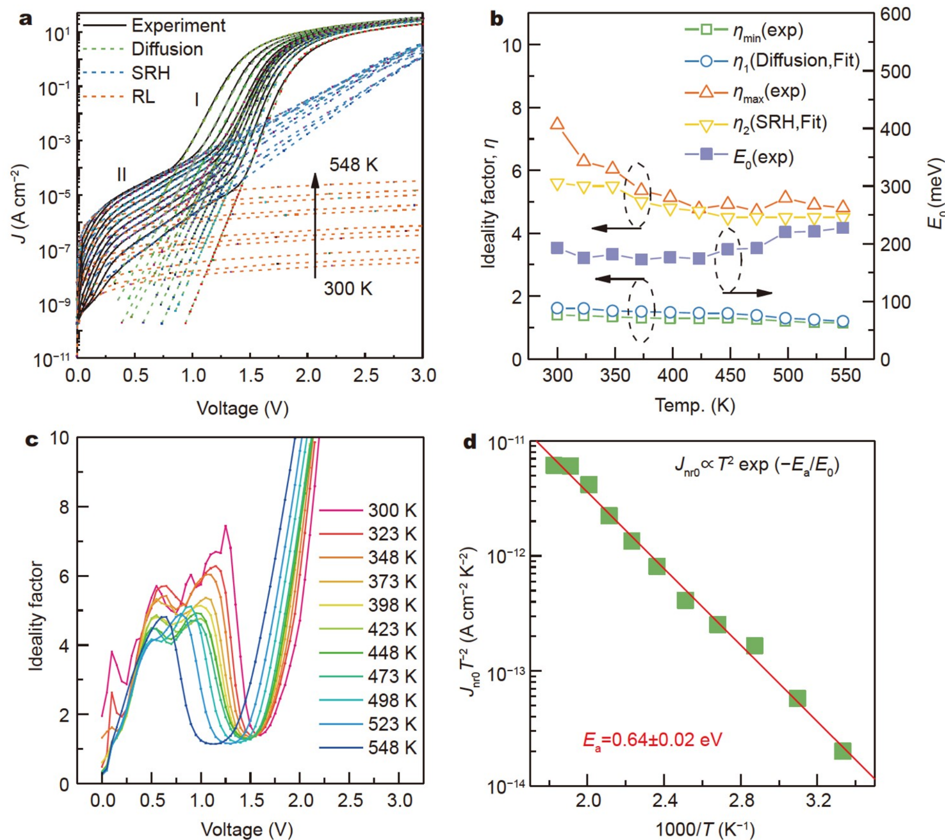

Figure 2 (a) Forward J-V-T characteristics (solid line) of HJD from 300 to 548 K. The dashed line is the fitting results of the model with multiple current mechanisms including diffusion, SRH recombination, and junction edge leakage current. (b) The extracted E_0 and η as a function of temperature. (c) The extracted η-V-T plots. (d) Arrhenius plot for J_{nr0} where a linear fit gives the activation energy E_a of 0.64 ± 0.02 eV.

 © Science China Press and Springer-Verlag GmbH Germany, part of Springer Nature 2022

Considering the series resistance effect, the J-V characteristics of a p-n junction diode are given by [26]

$$J = J_d + J_{SRH} + J_{RL},$$

$$J_d = J_s\left[\exp\left(\frac{q(V-JR_s)}{\eta_1 kT}\right)-1\right],$$

$$J_{SRH} = J_{nr0}\left[\exp\left(\frac{q(V-JR_s)}{\eta_2 kT}\right)-1\right],$$

$$J_{RL} = \frac{(V-JR_s)}{R_{sh}}, \quad (3)$$

where J_s, J_{nr0} are bias-insensitive terms of diffusion and recombination current densities, respectively, η_1 and η_2 are the ideality factors in region-I and II, respectively. The shunt resistance R_{sh} is calculated by $R_{sh} = dV/dJ$ [26]. The first term in Equation (3) represents the diffusion current density (J_d), the second term is the trap-assisted SRH recombination (J_{SRH}), and the third one is the junction edge leakage current density (J_{RL}). The dashed lines in Fig. 2a show the goodness of fits with three current components described in Equation (3) and the fitted parameters are summarized in Table S1. As plotted in Fig. 2b, the temperature-dependence of the fitted η_1 and η_2 values are well consistent with the experimental η_{min} in the diffusion region-I and η_{max} in the subthreshold region-II, respectively, verifying the validity of the employed quantitative modeling. Indeed, in the subthreshold region, J_{nr0} is much higher than the other two counterparts (J_s and J_{RL}), as given by [33]

$$J_{nr0} = J_{00}T^2\exp\left(-\frac{E_a}{E_0}\right), \quad (4)$$

where E_a is the trap-related thermal activation energy and J_{00} is the reduced saturation current. From the Arrhenius plot of $\ln(J_{nr0}/T^2)$ in Fig. 2d, E_a is extracted to be 0.64 eV, which is related to the thermally activated traps that participate in the TAT process.

Fig. 3a shows the reverse J-V-T characteristics of the HJD device. At low fields, the exponential increase in reverse current density with the applied bias was proven to be dominated by the thermionic-field emission (TFE) process [34]. At high biases, the reverse current density shows a weak bias dependence, which was also observed in AlGaN [35], GaN [36], and Ga_2O_3 [10,34]-based devices and has been widely accepted as the contribution of Poole-Frenkel emission (PFE). Furthermore, PFE has been also reported to govern the current transport in the AlGaN/GaN heterostructure at low reverse biases [37]. PFE can be considered as the field-enhanced thermal excitation of carriers from the trap states into the continuum of electronic states, e.g., conduction band, which can be expressed as [34,35,37]

$$J_{PF} = CE\exp\left(-\frac{q\left(\phi_T-\sqrt{qE/\pi\varepsilon_\infty\varepsilon_0}\right)}{kT}\right),$$

$$\text{or } \ln\left(\frac{J_{PE}}{E}\right) = m(T)\sqrt{E}+C(T),$$

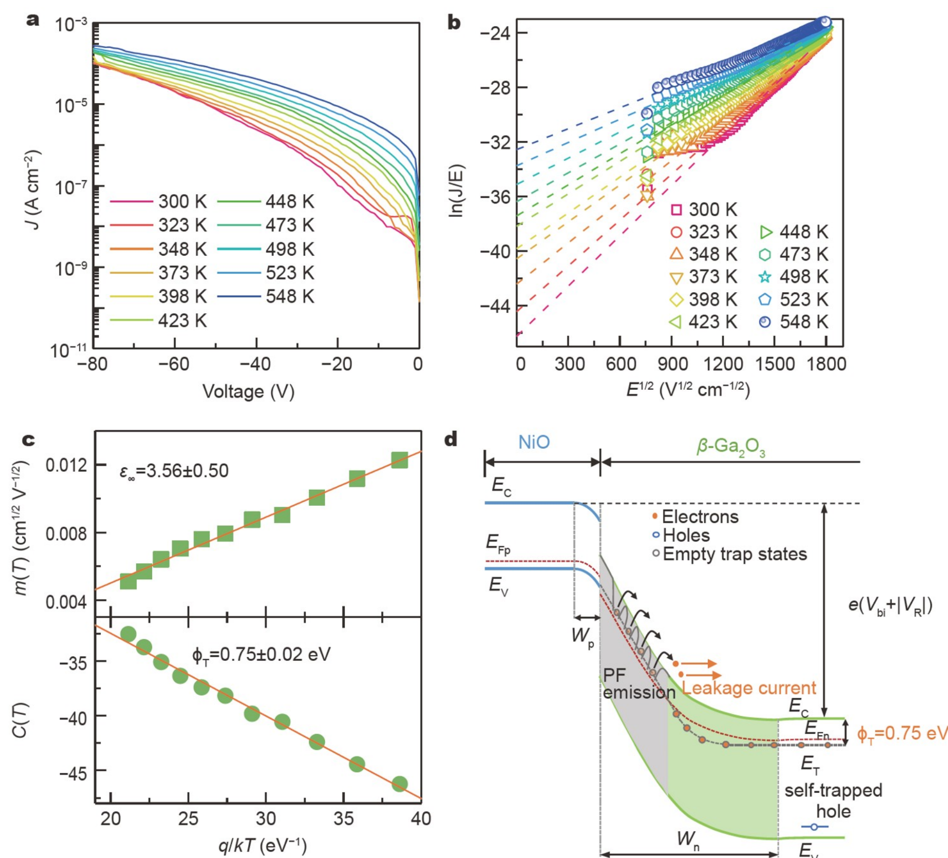

Figure 3 (a) Reverse J-V-T characteristics of HJD from 300 to 548 K. (b) Temperature-dependent $\ln(J/E)$-$E^{1/2}$ curves. Dash line represents good linear fit at high fields. (c) Arrhenius plots for $m(T)$ and $C(T)$, where a liner fit gives the ε_∞ of 3.56 ± 0.50 and the energy barrier ϕ_T of 0.75 ± 0.02 eV, respectively. (d) Schematic of PFE in an energy band diagram of the NiO/β-Ga_2O_3 heterojunction.

© Science China Press and Springer-Verlag GmbH Germany, part of Springer Nature 2022

$$m(T) = \frac{q}{kT}\sqrt{\frac{q}{\pi\varepsilon_0\varepsilon_\infty}},$$

$$C(T) = -\frac{q\phi_T}{kT} + \log C, \tag{5}$$

where $E = [2qN_D(V + V_{bi} - kT/q)\varepsilon_0\varepsilon_n]^{1/2}$ [38] is the electric field in the depletion region of β-Ga_2O_3, ε_∞ is the high-frequency dielectric permittivity of β-Ga_2O_3, ϕ_T is the barrier height for electron emission from the trap state, and C is a constant. The ln(J/E)-$E^{1/2}$ plots in Fig. 3b for all measured temperatures follow the expected linear evolution in high field regimes as predicted by Equation (5), which validates that PFE is the dominant contributor to the reverse leakage.

Through the linear fittings, a series of $m(T)$ and $C(T)$ are extracted from the slopes and y-axis intercepts in Fig. 3b, respectively. The Arrhenius plots of $m(T)$ and $C(T)$ *versus* q/kT are shown in Fig. 3c, respectively. The slope of an excellent linear fit between $m(T)$ and q/kT gives rise to $\varepsilon_\infty = 3.56 \pm 0.50$. This value is in good agreement with the reported high-frequency dielectric permittivity of β-Ga_2O_3 [39,40], which thus further validates the identification of the PFE model in this work. The slope of the linear fit of the Arrhenius plots of $C(T)$ gives rise to the energy barrier of traps of $\phi_T = 0.75 \pm 0.02$ eV below the conduction band. Fig. 3d schematically shows the energy band diagram under a high reverse bias. In the quasi-equilibrium state, traps under the Fermi level are occupied by electrons. At a high V_R, the depletion region in β-Ga_2O_3 is expanded with an enhanced electric field. As a result, electrons localized in the traps higher than the Fermi level will overcome barriers (ϕ_T) and be emitted to the conduction band through the PFE process. Subsequently, these electrons are quickly swept out of the depletion region, contributing to the reverse leakage current.

DISCUSSION

To explore the nature of traps related to the forward subthreshold TAT process and the PFE at high reverse biases, DLTS and ICTS measurements have been performed. Traps with different carrier emission time constants (τ) under the same lock-in frequency (f) will respond to the independent DLTS peak by temperature scanning, and thus, a series of trap signatures (τ_{max}, T_{max}) can be obtained by changing f, which is called DLTS [12,41]. Furthermore, a series of trap signatures that are more sensitive to frequency changes can be obtained by frequency scanning at a fixed temperature, which is known as ICTS [42]. In terms of the well-known equation of [12]

$$\ln(1/\tau T^2) = -(1/kT)E_T + \ln(\lambda\sigma). \tag{6}$$

The trap activation energy (E_T) and carrier capture cross section (σ) can be obtained from the slope and y-intercept of the Arrhenius plot of $\ln(1/\tau T^2)$-$1/kT$, respectively, where γ is a constant related to carrier velocity (v_{th}) and effective state den-

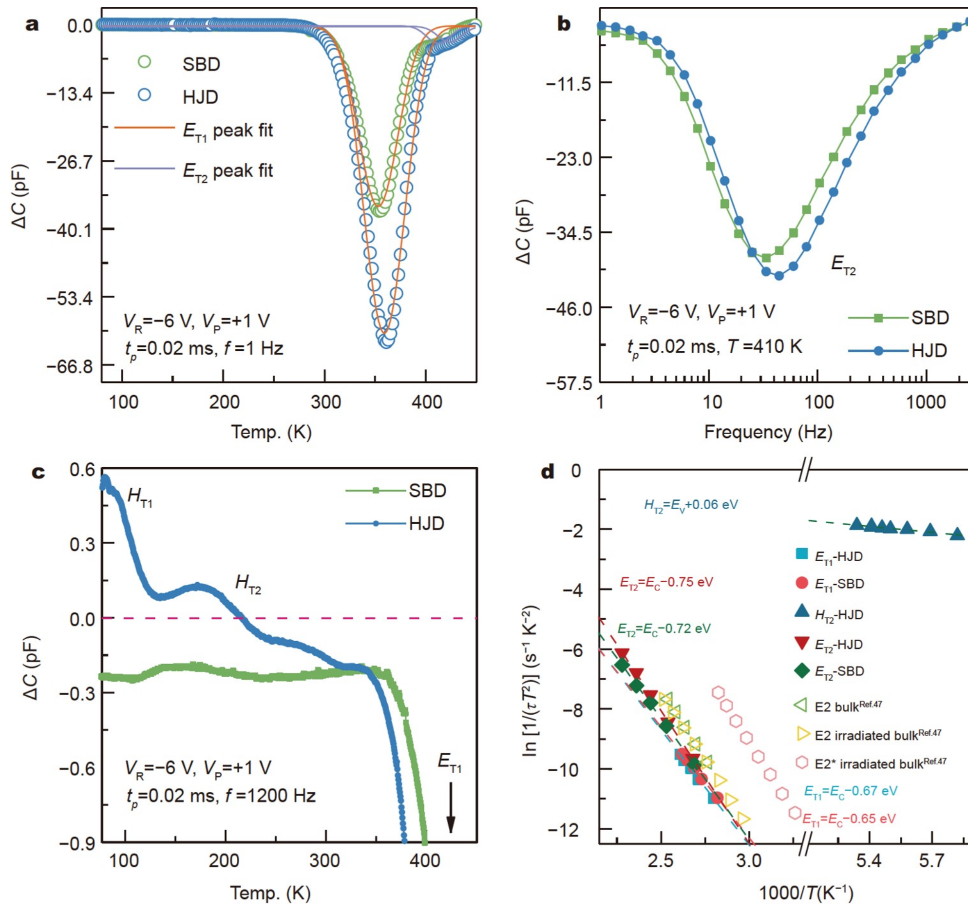

Figure 4 Fixed $V_R = -6$ V and $V_P = +1$ V, DLTS spectra of SBD and HJD recorded under conditions of (a) $t_p = 0.02$ ms, $f = 1$ Hz, and (c) $t_p = 0.02$ ms, $f = 1200$ Hz. (b) ICTS spectra of SBD and HJD recorded under the condition of $V_R = -6$ V, $V_P = +1$ V, $t_p = 0.02$ ms, $T = 410$ K and $f = 1$–2500 Hz. (d) Arrhenius plots of detected trap by this work (E_{T1}, E_{T2} and H_{T2}) and from Ingebrigtsen *et al.* [47] (E2 and E2*).

 © Science China Press and Springer-Verlag GmbH Germany, part of Springer Nature 2022

sity in conduction band or valence band. Fig. 4a shows the DLTS spectra of the SBD and HJD, which were recorded in the condition of a fixed reverse voltage $V_R = -6$ V, a pulse filling voltage $V_P = +1$ V, a pulse filling time $t_p = 0.02$ ms, and $f = 1$ Hz. Both diodes exhibit similar DLTS feature across the entire scanning temperature regions, which can be deconvoluted into a strong negative peak around 350 K and a weak shoulder peak near 410 K. For such a NiO/β-Ga_2O_3 p^+-n heterojunction, the transient capacitance detected by DLTS mainly comes from lightly doped β-Ga_2O_3 side and thus both DLTS peaks are corresponding to majority carrier (electron) traps in β-Ga_2O_3, which are named as E_{T1} and E_{T2}, respectively. To distinguish the E_{T2} trap states, the ICTS measurements were performed near the peak temperature of 410 K in the condition of $V_R = -6$ V, $V_P = +1$ V, $t_p = 0.02$ ms, $T = 410$ K and $f = 1$–2500 Hz. Fig. 4b shows that the peak intensity of E_{T2} traps revealed by ICTS is almost the same for the SBD and HJD, and is also consistent with the characteristics of E_{T2} in DLTS. It allows the accurate determination of E_{T2} trap properties.

To detect traps with different τ, the DLTS measurements were also performed in the condition of $f = 1200$ Hz and $t_p = 0.02$ ms and plotted in Fig. 4c. The DLTS signal for SBD remains negative regardless the changing frequency and shifted towards high temperature regime. In comparison, two additional positive DLTS peaks appear in the temperature region below 100 K and around 200 K at high frequency for the HJD bipolar device, which is a typical contribution by minority carrier (hole) traps, as named with H_{T1} and H_{T2} herein. It is expected that minority carrier injection is almost negligible in Schottky diodes that are the majority carrier devices. To exclude the artificial DLTS peaks caused by the carrier freezing-out effect, the temperature-dependent capacitance (*C-T*) characteristics of both diodes have been investigated in Fig. S2. Besides the obvious capacitance drop between 350 to 400 K contributed by the electron traps, another falling edge of capacitance appears around 200 K for both diodes, which indicates that carriers are partially frozen in β-Ga_2O_3 and p-NiO at low temperatures. Even so, no positive peak appears in the DLTS spectrum of the SBD, indicating that the partial carrier freezing at ~200 K will not affect the detection of H_{T2} traps in β-Ga_2O_3. The detection of H_{T2} in HJD results from the predictable hole injection from p^+-NiO to β-Ga_2O_3 in this bipolar device. Note that the recent electron beam-induced current (EBIC) [43,44] and optical DLTS (ODLTS) [45] experiments unanimously verified the mobile characteristics of holes in β-Ga_2O_3 at cryogenic temperature. Fig. S3 shows the V_R- and V_P-dependent DLTS spectra of HJD. The dependence of H_{T2}-peak on the electric field reflects the characteristics of bulk traps in β-Ga_2O_3 rather than interfacial traps distributed at the NiO/β-Ga_2O_3 hetero-interface [46]. In addition, the incomplete DLTS spectral shapes of the H_{T1} trap in Fig. 4c do not allow accurately evaluating its properties, and thus are not discussed in this work.

Fig. 4d shows the Arrhenius plots of the detected traps, including the results of the EFG bulk β-Ga_2O_3 reported by Ingebrigtsen *et al.* [47], where the comparison results indicate that both E_{T1} and E_{T2} exhibit similar properties to E2. The relevant fitted parameters are summarized in Table 1. For SBD and HJD, electron trap E_{T1} exhibits the energy level of $E_C - 0.65$ eV and $E_C - 0.67$ eV, the concentration (N_T) of 4.2×10^{16} and 9.1×10^{16} cm^{-3}, and σ of $(7–8) \times 10^{-18}$ and $(1–2) \times 10^{-17}$ cm^2, respectively. Meanwhile, E_{T2} detected by ICTS exhibits the energy level of $E_C - 0.72$ eV and $E_C - 0.75$ eV and trap concentration of 2.7×10^{17} and 2.9×10^{17} cm^{-3}, respectively, for SBD and HJD. Zimmermann *et al.* [48] reported that E2 contains two overlapping levels of E2a and E2b, where E2a ($E_C - 0.66$ eV) is related to Fe substituting for Ga on a tetrahedral site (Fe_{GaI}) and E2b ($E_C - 0.73$ eV) is related to Fe substituting for Ga on a octahedral site (Fe_{GaII}) in the EFG bulk β-Ga_2O_3. In comparison, the energy levels of traps E_{T1} and E_{T2} are quite consistent with that of E2a and E2b, and the capture cross section of E_{T1} is one order of magnitude lower than E_{T2}, which is also consistent with the difference between E2a and E2b [48]. The unintentional incorporation of Fe impurities in the EFG bulk β-Ga_2O_3 has been confirmed by the secondary ion mass spectroscopy (SIMS) measurement [47], and therefore, E_{T1} and E_{T2} traps most possibly originate from the Fe_{GaI} and Fe_{GaII} in the EFG bulk β-Ga_2O_3, respectively.

In addition, H_{T2} trap that was only detected in HJD shows a shallow energy level of $E_V + 0.06$ eV, a low concentration $N_{HT2} = 4.3 \times 10^{14}$ cm^{-3} and a small hole capture cross section $\sigma_{p2} = (1–2) \times 10^{-21}$ cm^2. It is possibly related to self-trapped holes (STHs), well aligned with the DLOS results [49,50]. With knowledge of trap properties, the correlation between carrier transport and trapping behaviors can be established. Surprisingly, as the E_{T1} level ($E_C - 0.67$ eV) is well consistent with the trap activation energy ($E_a = 0.64 \pm 0.02$ eV) obtained by the *J-V-T* characteristics, which implies that the dominant modified SRH recombination in the subthreshold conduction region of HJD is mainly mediated by E_{T1} traps related to Fe_{GaI}. Furthermore, the E_{T2} level in HJD is consistent with the carrier barrier height during the PFE process, which further confirms that the leakage path of the reverse current is related to high density of Fe.

CONCLUSIONS

Trap-mediated bipolar charge transport and its correlation to deep-level trap properties in NiO/β-Ga_2O_3 HJD have been investigated. The modified SRH recombination current mediated by E_{T1} ($E_C - 0.67$ eV) related to Fe_{GaI} has been verified to govern the forward subthreshold conduction, while the reverse leakage at high fields is dominated by PFE from bulk traps related to Fe_{GaII} ($E_C - 0.75$ eV). The established correlation between carrier transport, trapping, and recombination kinetics

Table 1 Summary of trap parameters detected by DLTS and ICTS

Traps	Device	Energy level (eV)	σ (cm^2)	N_T (cm^{-3})	Possible origins
E_{T1}	SBD	$E_C - 0.65$	$(7–8) \times 10^{-18}$	4.2×10^{16}	Fe_{GaI}
E_{T1}	HJD	$E_C - 0.67$	$(1–2) \times 10^{-17}$	9.1×10^{16}	Fe_{GaI}
E_{T2}	SBD	$E_C - 0.72$	$(6–7) \times 10^{-17}$	2.7×10^{17}	Fe_{GaII}
E_{T2}	HJD	$E_C - 0.75$	$(3–4) \times 10^{-16}$	2.9×10^{17}	Fe_{GaII}
H_{T2}	HJD	$E_V + 0.06$	$(1–2) \times 10^{-21}$	4.3×10^{14}	STHs

© Science China Press and Springer-Verlag GmbH Germany, part of Springer Nature 2022

in the NiO/β-Ga_2O_3 heterojunction is crucial for the interface engineering of high-performance Ga_2O_3 bipolar power devices.

Received 5 July 2022; accepted 5 September 2022; published online 25 November 2022

1 Pearton SJ, Yang J, Cary Iv PH, *et al.* A review of Ga_2O_3 materials, processing, and devices. Appl Phys Rev, 2018, 5: 011301
2 Zhang J, Shi J, Qi DC, *et al.* Recent progress on the electronic structure, defect, and doping properties of Ga_2O_3. APL Mater, 2020, 8: 020906
3 Hao W, He Q, Zhou X, *et al.* 2.6 kV NiO/Ga_2O_3 heterojunction diode with superior high-temperature voltage blocking capability. In: 2022 IEEE 34th International Symposium on Power Semiconductor Devices and ICs (ISPSD). Vancouver, BC, 2022, 105–108
4 Zhou X, Liu Q, Hao W, *et al.* Normally-off β-Ga_2O_3 power heterojunction field-effect-transistor realized by p-NiO and recessed-gate. In: 2022 IEEE 34th International Symposium on Power Semiconductor Devices and ICs (ISPSD). Vancouver, BC, 2022, 101–104
5 Zhang J, Dong P, Dang K, *et al.* Ultra-wide bandgap semiconductor Ga_2O_3 power diodes. Nat Commun, 2022, 13: 3900
6 Gong H, Chen X, Xu Y, *et al.* Band alignment and interface recombination in NiO/β-Ga_2O_3 type-II p-n heterojunctions. IEEE Trans Electron Devices, 2020, 67: 3341–3347
7 Gong HH, Chen XH, Xu Y, *et al.* A 1.86-kV double-layered NiO/β-Ga_2O_3 vertical p-n heterojunction diode. Appl Phys Lett, 2020, 117: 022104
8 Kokubun Y, Kubo S, Nakagomi S. All-oxide p-n heterojunction diodes comprising p-type NiO and n-type β-Ga_2O_3. Appl Phys Express, 2016, 9: 091101
9 Watahiki T, Yuda Y, Furukawa A, *et al.* Heterojunction p-Cu_2O/n-Ga_2O_3 diode with high breakdown voltage. Appl Phys Lett, 2017, 111: 222104
10 Gong HH, Yu XX, Xu Y, *et al.* β-Ga_2O_3 vertical heterojunction barrier Schottky diodes terminated with p-NiO field limiting rings. Appl Phys Lett, 2021, 118: 202102
11 Gong H, Zhou F, Xu W, *et al.* 1.37 kV/12 A NiO/β-Ga_2O_3 heterojunction diode with nanosecond reverse recovery and rugged surge-current capability. IEEE Trans Power Electron, 2021, 36: 12213–12217
12 Schroder DK. Semiconductor Material and Device Characterization. New York: John Wiley & Sons, 2005, 151–165
13 De Santi C, Fregolent M, Buffolo M, *et al.* Carrier capture kinetics, deep levels, and isolation properties of β-Ga_2O_3 Schottky-barrier diodes damaged by nitrogen implantation. Appl Phys Lett, 2020, 117: 262108
14 McGlone JF, Xia Z, Joishi C, *et al.* Identification of critical buffer traps in Si δ-doped β-Ga_2O_3 MESFETs. Appl Phys Lett, 2019, 115: 153501
15 Mcglone JF, Xia Z, Zhang Y, *et al.* Trapping effects in Si δ-doped β-Ga_2O_3 MESFETs on an Fe-doped β-Ga_2O_3 substrate. IEEE Electron Device Lett, 2018, 39: 1042–1045
16 Zhang KHL, Wu R, Tang F, *et al.* Electronic structure and band alignment at the NiO and $SrTiO_3$ p-n heterojunctions. ACS Appl Mater Interfaces, 2017, 9: 26549–26555
17 Schein FL, von Wenckstern H, Grundmann M. Transparent p-CuI/n-ZnO heterojunction diodes. Appl Phys Lett, 2013, 102: 092109
18 Grundmann M, Klüpfel F, Karsthof R, *et al.* Oxide bipolar electronics: Materials, devices and circuits. J Phys D-Appl Phys, 2016, 49: 213001
19 Kaushik JK, Balakrishnan VR, Panwar BS, *et al.* On the origin of kink effect in current-voltage characteristics of AlGaN/GaN high electron mobility transistors. IEEE Trans Electron Devices, 2013, 60: 3351–3357
20 Tress W, Corvers S, Leo K, *et al.* Investigation of driving forces for charge extraction in organic solar cells: Transient photocurrent measurements on solar cells showing S-shaped current-voltage characteristics. Adv Energy Mater, 2013, 3: 873–880
21 Wang Y, Gong H, Lv Y, *et al.* 2.41 kV vertical p-NiO/n-Ga_2O_3 heterojunction diodes with a record Baliga's figure-of-merit of 5.18 GW/cm^2. IEEE Trans Power Electron, 2022, 37: 3743–3746
22 Palmer DW. Characterisation of semiconductor heterostructures by capacitance methods. Microelectron J, 1999, 30: 665–672
23 Passlack M, Schubert EF, Hobson WS, *et al.* Ga_2O_3 films for electronic and optoelectronic applications. J Appl Phys, 1995, 77: 686–693
24 Rao KV, Smakula A. Dielectric properties of cobalt oxide, nickel oxide, and their mixed crystals. J Appl Phys, 1965, 36: 2031–2038
25 Mandurrino M, Goano M, Vallone M, *et al.* Semiclassical simulation of trap-assisted tunneling in GaN-based light-emitting diodes. J Comput Electron, 2015, 14: 444–455
26 Alialy S, Tecimer H, Uslu H, *et al.* A comparative study on electrical characteristics of Au/N-Si Schottky diodes, with and without Bi-doped PVA interfacial layer in dark and under illumination at room temperature. J Nanomed Nanotechnol, 2017, 04: 1000167
27 Zhu D, Xu J, Noemaun AN, *et al.* The origin of the high diode-ideality factors in GaInN/GaN multiple quantum well light-emitting diodes. Appl Phys Lett, 2009, 94: 081113
28 Hu Z, Nomoto K, Song B, *et al.* Near unity ideality factor and Shockley-Read-Hall lifetime in GaN-on-GaN p-n diodes with avalanche breakdown. Appl Phys Lett, 2015, 107: 243501
29 Grundmann M, Karsthof R, von Wenckstern H. Interface recombination current in type II heterostructure bipolar diodes. ACS Appl Mater Interfaces, 2014, 6: 14785–14789
30 Yan D, Lu H, Chen D, *et al.* Forward tunneling current in GaN-based blue light-emitting diodes. Appl Phys Lett, 2010, 96: 083504
31 Ma N, Tanen N, Verma A, *et al.* Intrinsic electron mobility limits in β-Ga_2O_3. Appl Phys Lett, 2016, 109: 212101
32 Auf der Maur M, Galler B, Pietzonka I, *et al.* Trap-assisted tunneling in InGaN/GaN single-quantum-well light-emitting diodes. Appl Phys Lett, 2014, 105: 133504
33 Bozyigit D, Lin WMM, Yazdani N, *et al.* A quantitative model for charge carrier transport, trapping and recombination in nanocrystal-based solar cells. Nat Commun, 2015, 6: 6180
34 Xu Y, Chen X, Zhou D, *et al.* Carrier transport and gain mechanisms in β-Ga_2O_3-based metal-semiconductor-metal solar-blind Schottky photodetectors. IEEE Trans Electron Devices, 2019, 66: 2276–2281
35 Rathkanthiwar S, Kalra A, Solanke SV, *et al.* Gain mechanism and carrier transport in high responsivity AlGaN-based solar blind metal semiconductor metal photodetectors. J Appl Phys, 2017, 121: 164502
36 Rao PK, Park B, Lee ST, *et al.* Analysis of leakage current mechanisms in Pt/Au Schottky contact on Ga-polarity GaN by Frenkel-Poole emission and deep level studies. J Appl Phys, 2011, 110: 013716
37 Greco G, Fiorenza P, Spera M, *et al.* Forward and reverse current transport mechanisms in tungsten carbide Schottky contacts on AlGaN/GaN heterostructures. J Appl Phys, 2021, 129: 234501
38 Tomer D, Rajput S, Hudy LJ, *et al.* Carrier transport in reverse-biased graphene/semiconductor Schottky junctions. Appl Phys Lett, 2015, 106: 173510
39 Liu B, Gu M, Liu X. Lattice dynamical, dielectric, and thermodynamic properties of β-Ga_2O_3 from first principles. Appl Phys Lett, 2007, 91: 172102
40 Rebien M, Henrion W, Hong M, *et al.* Optical properties of gallium oxide thin films. Appl Phys Lett, 2002, 81: 250–252
41 Wang Z, Chen X, Ren FF, *et al.* Deep-level defects in gallium oxide. J Phys D-Appl Phys, 2021, 54: 043002
42 Okushi H, Tokumaru Y. Isothermal capacitance transient spectroscopy for determination of deep level parameters. Jpn J Appl Phys, 1980, 19: L335–L338
43 Lee J, Flitsiyan E, Chernyak L, *et al.* Effect of 1.5 MeV electron irradiation on β-Ga_2O_3 carrier lifetime and diffusion length. Appl Phys Lett, 2018, 112: 082104
44 Yakimov EB, Polyakov AY, Smirnov NB, *et al.* Diffusion length of non-equilibrium minority charge carriers in β-Ga_2O_3 measured by electron beam induced current. J Appl Phys, 2018, 123: 185704
45 Polyakov AY, Smirnov NB, Shchemerov IV, *et al.* Hole traps and persistent photocapacitance in proton irradiated β-Ga_2O_3 films doped with Si. APL Mater, 2018, 6: 096102
46 Coelho AVP, Adam MC, Boudinov H. Distinguishing bulk traps and interface states in deep-level transient spectroscopy. J Phys D-Appl Phys, 2011, 44: 305303
47 Ingebrigtsen ME, Varley JB, Kuznetsov AY, *et al.* Iron and intrinsic deep level states in Ga_2O_3. Appl Phys Lett, 2018, 112: 042104
48 Zimmermann C, Frodason YK, Barnard AW, *et al.* Ti- and Fe-related

 © Science China Press and Springer-Verlag GmbH Germany, part of Springer Nature 2022

charge transition levels in β-Ga_2O_3. Appl Phys Lett, 2020, 116: 072101
49 Farzana E, Ahmadi E, Speck JS, *et al.* Deep level defects in Ge-doped (010) β-Ga_2O_3 layers grown by plasma-assisted molecular beam epitaxy. J Appl Phys, 2018, 123: 161410
50 Zhang Z, Farzana E, Arehart AR, *et al.* Deep level defects throughout the bandgap of (010) β-Ga_2O_3 detected by optically and thermally stimulated defect spectroscopy. Appl Phys Lett, 2016, 108: 052105

Acknowledgements This work was financially supported by the National Key R&D Program of China (2022YFB3605400), the State Key Research and Development Project of Guangdong (2020B010174002), and the National Natural Science Foundation of China (62234007, U21A20503 and U21A2071).

Author contributions Wang Z performed the device fabrication and characterizations; Wang Z and Ye J analyzed the results and wrote the paper. All authors contributed to the discussion and revised the manuscript.

Conflict of interest The authors declare that they have no conflict of interest.

Supplementary information Supporting data are available in the online version of the paper.

Zhengpeng Wang is a PhD candidate at the School of Electronic Science and Engineering, Nanjing University, China. His research is focusing on the power device physics and defect engineering.

Jiandong Ye holds the full professorship of the School of Electronic Science and Engineering at Nanjing University, China. He is engaged in the material, physics and devices of wide-bandgap semiconductors.

NiO/Ga_2O_3 p^+-n异质结功率二极管中陷阱介导双极型电荷输运研究

汪正鹏[1], 巩贺贺[1], 郁鑫鑫[1], 纪晓丽[1], 任芳芳[1], 杨燚[1], 顾书林[1], 郑有炓[1], 张荣[1], 叶建东[1,2*]

摘要 构筑NiO/Ga_2O_3 p^+-n异质结是克服Ga_2O_3 p型掺杂瓶颈从而实现双极型功率电子器件的有效途径, 然而限制器件性能的缺陷行为与双极型电荷输运等物理机制尚不明晰. 本论文研究了NiO/Ga_2O_3 p^+-n异质结中陷阱介导的载流子输运、俘获和复合动力学之间的内在关联特性. 变温电流-电压特性的量化分析表明, 在正偏亚阈值区, 陷阱辅助隧穿占据主导地位, 符合多数载流子陷阱介导的Shockley-Read-Hall复合模型, 其陷阱激活能为0.64 eV, 与深能级瞬态谱测试的陷阱能级位置(E_C − 0.67 eV)非常吻合; 当正向偏压大于器件开启电压时, 器件输运特性由少数载流子扩散所主导, 器件理想因子接近于1. 在反向偏置的高场作用下, 器件漏电机制则由β-Ga_2O_3体材料中的陷阱引起的Poole-Frenkel (PF)发射所导致. PF发射的势垒高度为0.75 eV, 与等温变频深能级瞬态谱测得的陷阱能级位置(E_C − 0.75 eV)相一致. 这一工作有助于建立NiO/Ga_2O_3 p^+-n异质结中双极型电荷输运和深能级缺陷行为间的内在关联, 对理解和发展Ga_2O_3双极型功率整流器件具有重要的参考价值.

 © Science China Press and Springer-Verlag GmbH Germany, part of Springer Nature 2022